Mesospheric temperature and circulation response to the Hunga Tonga-Hunga-Ha'apai volcanic eruption

Wandi Yu[1], Rolando R. Garcia[2], Jia Yue[3,4], Anne K. Smith[2], Xinyue Wang[2], William J. Randel[2], Zishun Qiao[5],Yunqian Zhu[6,7],V.Lynn Harvey[6,8],Simone Tilmes[2], Martin G. Mlynczak[9]

[1]Department of Atmospheric and Planetary Sciences, Hampton University, Hampton, VA, USA
[2]Atmospheric Chemistry Observations & Modeling, National Center for Atmospheric Research, Boulder, CO, USA
[3]NASA Goddard Space Flight Center, Greenbelt, MD, USA
[4]Catholic University of America, Washington, DC, USA
[5]Embry-Riddle Aeronautical University, FL, USA
[6]Laboratory for Atmospheric and Space Physics, University of Colorado Boulder, Boulder, USA
[7]University of Colorado Cooperative Institute for Research in Environmental Sciences (CIRES) at the NOAA Chemical Sciences Laboratory, Boulder, CO, USA
[8]Atmospheric and Oceanic Sciences Department, University of Colorado, Boulder, CO, USA
[9]NASA Langley Research Center, Hampton, VA, USA

Key Points:

- SABER observed unprecedented mesospheric temperature variations in the Southern Hemisphere in August 2022 after the HTHH eruption.
- WACCM simulations indicate that changes in the mesospheric temperature are due to a stronger mesospheric meridional circulation.
- Stronger stratospheric westerlies after eruption enhance westward gravity wave drag in the mesosphere, thus a stronger circulation.

Corresponding author: Wandi Yu, wandi.yu@hamptonu.edu

Abstract

The Hunga Tonga Hunga-Ha'apai (HTHH) volcanic eruption on 15 January 2022 injected water vapor and SO_2 into the stratosphere. Several months after the eruption, significantly stronger westerlies, and a weaker Brewer-Dobson circulation developed in the stratosphere of the Southern Hemisphere and were accompanied by unprecedented temperature anomalies in the stratosphere and mesosphere. In August 2022 the Sounding of the Atmosphere using Broadband Emission Radiometry (SABER) satellite instrument observed record-breaking temperature anomalies in the stratosphere and mesosphere that alternate signs with altitude. Ensemble simulations carried out with the Whole Atmosphere Community Climate Model (WACCM6) indicate that the strengthening of the stratospheric westerlies explains the mesospheric temperature changes. The stronger westerlies cause stronger westward gravity wave drag in the mesosphere, accelerating the mesospheric mean meridional circulation. The stronger mesospheric circulation, in turn, plays a dominant role in driving the changes in mesospheric temperatures. This study highlights the impact of large volcanic eruptions on middle atmospheric dynamics and provides insight into their long-term effects in the mesosphere. On the other hand, we could not discern a clear mechanism for the observed changes in stratospheric circulation. In fact, an examination of the WACCM ensemble reveals that not every member reproduces the large changes observed by SABER. We conclude that there is a stochastic component to the stratospheric response to the HTHH eruption.

Plain Language Summary

This work studies the impact of the Hunga Tonga-Hunga Ha'apai volcanic eruption, which took place on January 15, 2022, on the earth's mesosphere (55 km – 80 km). The eruption injected water vapor and SO_2 into the stratosphere, which was followed by changes in the wind patterns in the stratosphere (16 km – 55 km). Concurrent with these changes, we observed unprecedented temperature changes in the mesosphere, with record high and low temperature anomalies in August that alternate signs with altitude. We used climate model simulations to show that the changes in stratospheric winds were ultimately responsible for these record-breaking mesospheric temperatures. We found that the stronger winds in the stratosphere enhanced gravity wave breaking in the mesosphere, which led to changes in the circulation and thus the temperature. However, we could not find a clear mechanism for the changes observed in the stratosphere.

1 Introduction

On 15 January 2022, a submarine volcano erupted in Hunga Tonga - Hunga Ha'apai (HTHH, 20.54°S, 175.38°W). The volcanic plume reached 55-57 km (Carn et al., 2022; Proud et al., 2022). This eruption injected $\sim$ 50-150 Tg of water vapor into the stratosphere and increased the total stratospheric water vapor burden by 5-13% reported by different observational instruments (Khaykin et al., 2022; Millán et al., 2022; Randel et al., 2023; Vömel et al., 2022) Meanwhile, 0.4-0.5 Tg of SO_2 was also injected into the stratosphere (Carn et al., 2022), and formed sulfate aerosols (Khaykin et al., 2022; Taha et al., 2022; Zhu et al., 2022).

The HTHH volcanic eruption changed the dynamics in the stratosphere. In the few months following the eruption, the injected water vapor cooled the middle stratosphere and warmed the lower stratosphere; and the sulfate aerosol formed from the injected SO_2 warmed the lower stratosphere (Schoeberl et al., 2022; Sellitto et al., 2022; Wang et al., 2022). These warming and cooling patterns coincide with the distribution of water vapor and sulfate aerosol. However, in the austral winter of 2022, the stratospheric westerly jet shifted equatorward and strengthened, concurrent with a weakening of the stratospheric Brewer-Dobson circulation (Coy et al., 2022; Wang et al., 2022), leading to a depletion of ozone in the mid-latitudes (Wang et al., 2022). At this time, the temperature

anomalies consistent with the changes in the stratospheric jet no longer coincided with the location of the water vapor and aerosol anomalies.

The mesosphere is the layer of the atmosphere above the stratosphere, from ∼50 km to ∼85 km, or about 1 hPa to 0.01 hPa. The mesospheric temperature can be envisaged as being composed of the global mean vertical profile, determined by radiative equilibrium, plus local departures determined mainly by dynamical processes (Andrews et al., 1987). The mesospheric meridional circulation is the most important dynamical process that transports heat and chemical species (Randall et al., 2009; Smith et al., 2011, 2010). It is composed of a single, inter-hemispheric cell, with ascent in the summer hemisphere and descent in the winter hemisphere, connected by cross-equatorial flow from the summer hemisphere to the winter hemisphere. The circulation is strongest near the two solstices (Dunkerton, 1978). Gravity waves propagating from below, some filtered out by the winds in the stratosphere, break in the mesosphere and deposit angular momentum that drives the mesospheric circulation (Andrews et al., 1987; Garcia & Solomon, 1985; Holton, 1983; Lindzen, 1981; Vincent, 2015). The gravity wave breaking that drives the mean meridional circulation is also referred to as "gravity wave drag".

The present study examines the impact of the HTHH volcanic eruption on the middle atmosphere, focusing specifically on changes in temperature and circulation in the mesosphere. By analyzing both satellite observations and model simulations, we aim to address several scientific questions. These include: (1) How does the mesospheric temperature respond to the HTHH volcanic eruption? (2) What is the relationship between changes in temperature and the mesospheric circulation that follow the eruption? and (3) What mechanisms contribute to the changes in mesospheric circulation following the eruption? We also discuss our attempts to understand the changes in stratospheric dynamics following the eruption, whose origin remains unclear.

2 Data and Model

The Sounding of the Atmosphere using Broadband Emission Radiometry (SABER) instrument onboard NASA's TIMED (Thermosphere Ionosphere Mesosphere Energetics Dynamics) satellite has been measuring temperature and chemical species in the middle atmosphere since January 2002 (Russell et al., 1999). To prevent the SABER detector from pointing directly at the Sun, TIMED performs a "yaw maneuver" that switches coverage from 83°S - 53°N to 83°N - 53°S every 60 days. SABER temperature data was validated by Dawkins et al. (2018), García-Comas et al. (2008), and Remsberg et al. (2008), and the stability of SABER calibration was examined by Mlynczak et al. (2020). The SABER temperature product covers the altitude range from the tropopause (∼17 km) to 110 km. In the mesosphere, the SABER temperature product has a vertical resolution of about 2 km, and we grid it into 5° latitude by 10° longitude bins. We use v2.07 of the SABER temperature product before December 2019, and v2.08 thereafter (Mlynczak et al., 2023). We use SABER temperature from 2003 to 2022, to avoid the possibility of errors due to the icing on the detector in the first year of operation (Remsberg et al., 2008).

We use NCAR's Whole Atmosphere Community Climate Model (WACCM6; Gettelman et al., 2019) to analyze the dynamic response of the stratosphere and mesosphere to volcanic eruption. This version of WACCM has 70 vertical layers and a horizontal resolution of 0.95° latitude by 1.25° longitude. We carried out two sets of experiments, each with 10 ensemble members. In the control ensemble, we nudge the temperature and wind field to the GEOS5 meteorological analysis data (Rienecker et al., 2018) throughout January 2022 until the beginning of February. The only difference between the ensemble members is that nudging ends on slightly different dates, in the range from 27 January 2022 to 5 February 2022. Once nudging end, the model runs freely and fully coupled to the ocean, sea-ice, and land. The volcanic eruption ensemble applies the same settings as

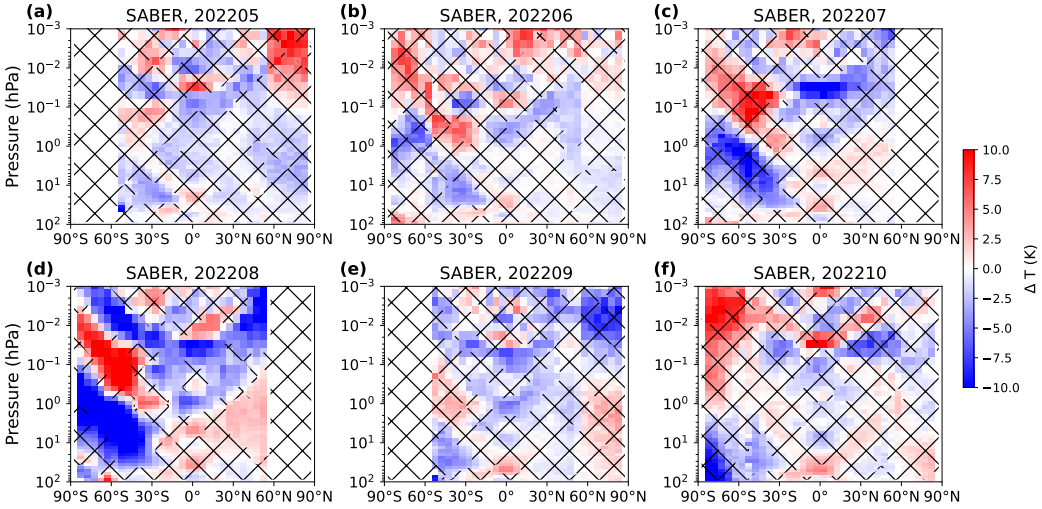

Figure 1. Monthly mean zonal mean temperature anomalies (2022 minus climatology) observed by SABER; the areas without hatching meet two thresholds: (1) must be outside of previous SABER variability and (2) exceed two standard deviations from the climatology. The plots cover the period from May to October 2022.

the control group but with the addition of the volcanic forcings. We inject 150 Tg of water vapor and 0.42 Tg SO_2 on January 15 following Zhu et al. (2022). Wang et al. (2022) have already demonstrated that this model setting successfully reproduces satellite observations of stratospheric dynamics following the HTHH volcanic eruption.

3 Results

The middle atmospheric temperature observed by SABER in 2022 displayed significant anomalies compared to the climatology of the previous 20 years of observations. Positive and negative anomalies in mesospheric temperature that exceeded both the high or low values in the historical record and two standard deviations from the climatological mean were occasionally observed, as shown in Fig. 1 (areas not covered by hatching). Some 2022 temperatures can be record-breaking but within 2 sigmas of the climatological mean, while some can exceed the 2-sigma threshold but not be record-breaking. Thus, we use both criteria jointly as an indication of statistical significance. The peak temperature anomalies occurred in July and August, revealing a tripolar pattern characterized by a cold center in the Southern Hemisphere (SH) extratropical stratosphere, a warm center in the mid-latitude mesosphere, and V-shaped cold anomalies extending from the lower mesosphere in the tropics to the upper mesosphere in the extratropics in both hemispheres, as shown in Fig. 1c-d. Notably, in August 2022, the mesospheric temperature in the tripolar structure reached record lows or highs for the entire SABER era (2003-2022). The August temperature anomalies are as large as ± 10 K in the stratosphere and mesosphere. This tripolar structure weakens in September and the significant anomalies dissipate after September 2022. We compared SABER temperature anomalies with those from the Microwave Limb Sounder (MLS, Livesey et al., 2020; Waters et al., 2006) v5.0 temperature product (not shown), which has a better vertical resolution in the stratosphere and has global coverage but a coarser vertical resolution in the mesosphere, and draw the same conclusion.

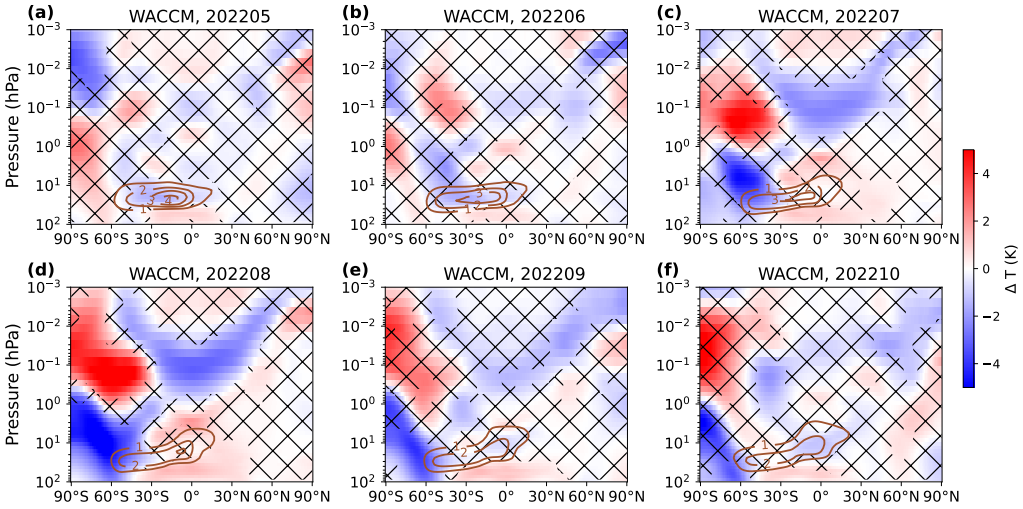

Figure 2. The 10-ensemble mean monthly mean zonal mean temperature difference between the volcano run and the control run in WACCM. The areas with differences that have a p-value > 0.05 in a Student's t-test are indicated by hatching. The plots cover the period from May to October 2022. Brown contours show zonal mean water vapor mixing ratio anomalies in ppmv.

To untangle the influence of the volcanic eruption from internal variability on changes in mesospheric temperature, we performed WACCM simulations where the only difference with respect to the control ensemble is whether H_2O and SO_2 are injected. We ran fully coupled free-running WACCM after February 2022 to capture the interaction between composition and circulation. In Fig. 2, we show the temperature difference (ΔT) between the ensemble means of the WACCM volcano case and the control case. The ensemble mean ΔT (the difference between the volcanic and control ensemble means) increased over time, exhibiting the same significant tripolar structure as that observed by SABER in July and August, with the structure weakening after September. The modeled ensemble mean ΔT pattern mirrors the observed tripolar structure. The magnitude of the ensemble-average signal is, however, 40% of that seen in the observations.

We examined the members of the volcanic ensemble individually for August 2022, comparing each one against the mean of the control ensemble. All ten volcanic ensemble members reproduce the observed temperature anomaly pattern in that month; six out of ten have an anomaly amplitude comparable to the observations (Figs. 3g-i and 3k-m); and four show a smaller amplitude (Figs. 3d-f and 3j). We refer to the six cases with a signal amplitude that is comparable to observations as "strong" cases, and to the other four cases as "weak" cases. The strong and weak cases occur independently of the date when nudging was stopped. The ensemble mean of the strong cases shows a significant tripolar structure with magnitudes comparable to the observations, with a maximum ΔT of $\pm$ 10 K in the stratosphere and mesosphere (Fig. 3c). These results may be summarized as follows: (1) all ten cases can reproduce the observed spatial structure indicating that the HTHH forcing is very likely the cause of the observed anomaly; and (2) a substantial fraction (40%) of the volcanic eruption simulations has a weak signal, indicating that there is a substantial stochastic component, such that the observed response is likely but not entirely deterministic.

We attempted to find a mechanistic explanation for the stratospheric temperature anomalies that develop in the months following the eruption but were unable to do so. At the same time when strong stratospheric temperature anomalies occur, there is a stronger

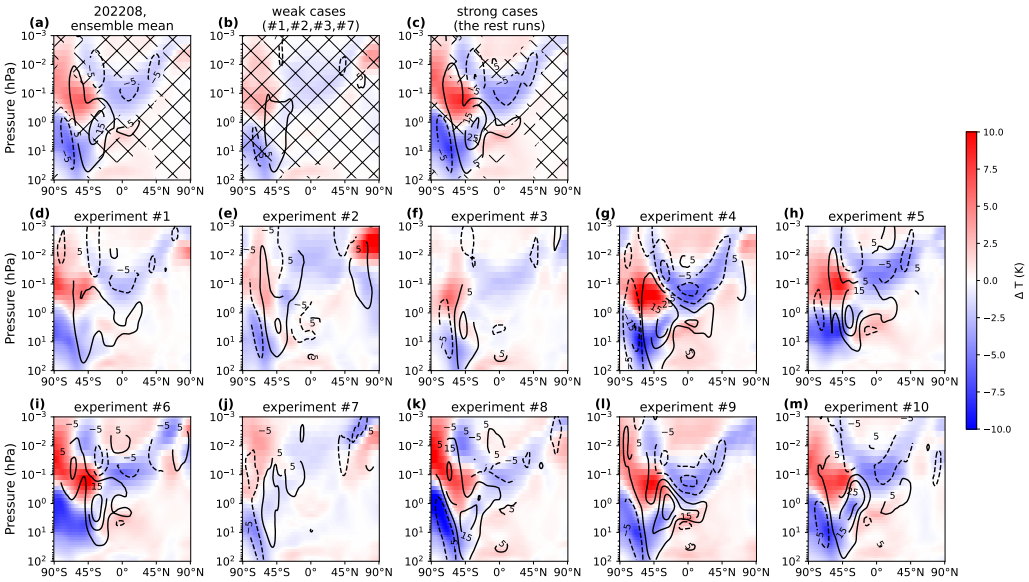

Figure 3. August 2022 zonal mean temperature difference (shading) between the volcano run and the ensemble mean control run in WACCM averaged over (a) all 10 volcanic ensemble members, (b) volcanic weak cases (case numbers 4,5,7), and (c) volcanic strong cases (the remainder of the cases in the volcanic ensemble). The areas with differences that have a p-value > 0.05 in a t-test are indicated by hatching. (d-m) The zonal mean temperature difference and zonal wind difference (contour) between each volcano run and the ensemble mean control run in WACCM. The date when nudging ends in WACCM is 27 January 2022 to 5 February 2022 in cases 1-10, respectively.

polar jet, a weakening in the planetary wave amplitude (mostly zonal wave 1), and thus weakening planetary wave drag (EP flux divergence) over SH mid-latitudes. This is a pattern of natural internal variability has been described in previous studies (e.g. Holton & Mass, 1976; Randel & Newman, 1998). We investigated the role of possible precursors to this pattern, in the months immediately following the eruption and before June, but we did not find statistically significant differences among the August strong and weak cases. The precursors we examined include radiative forcing from water vapor or sulfate aerosols, gravity wave drag, planetary wave propagation conditions, EP flux and EP flux divergence, meridional and zonal wind, and tropical and subtropical temperatures. We also examined the behavior of the quasi-biennial oscillation and found no statistically significant differences in amplitude or phase. Furthermore, we found that the strong and weak cases in July but are not always the same as the strong and weak cases in August. Finally, we have identified similar patterns of stratospheric temperature anomalies, although with somewhat weaker amplitude (within $\pm$ 7 K), to those observed in August in three control cases where no volcanic forcing is present. We conclude from these WACCM6 simulations that the strong July/August response in stratospheric temperature is partly stochastic, although the volcanic forcing (H_2O+SO_2) significantly increases the probability that the system will develop the observed SH system.

In contrast to the stratosphere, it is relatively simple to understand mechanistically the development of mesospheric temperature anomalies once the stratospheric changes are in place. In what follows, we focus on August 2022, the month with the strongest temperature response in both the stratosphere and mesosphere. We partition the meso-

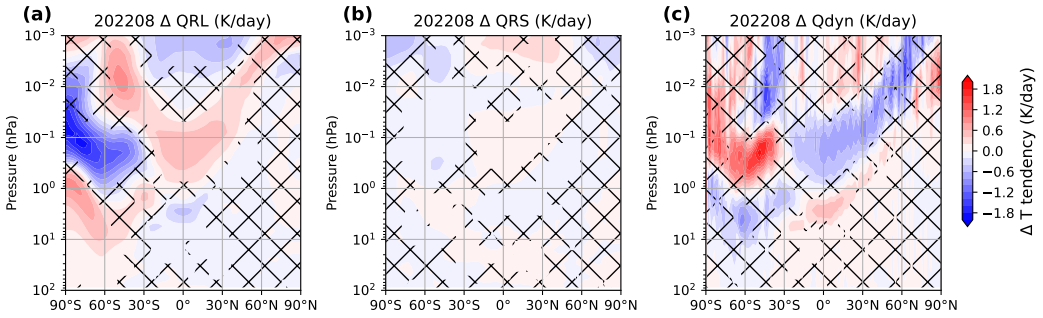

Figure 4. Latitude-pressure distribution of terms in the zonal-mean temperature budget in WACCM in August of 2022. The plots show the 10-member ensemble mean difference between the volcano case and the control case for (a) longwave heating rate, (b) shortwave heating rate, and (c) heating rate related to dynamics. The areas with differences that have a p-value > 0.05 in a t-test are indicated by hatching.

spheric temperature budget into contributions from radiation and dynamics, using the transformed Eulerian mean (TEM) thermodynamic equation (Andrews et al., 1987):

$$\frac{\partial \bar{T}}{\partial t} = -w^* S - v^* \frac{\partial \bar{T}}{a \partial \phi} + QRL + QRS \tag{1}$$

Where $\frac{\partial \bar{T}}{\partial t}$ is the rate of temperature change, v^* and w^* are the TEM meridional and vertical velocities, S is the static stability, QRL and QRS are the longwave and shortwave heating rates, a is the Earth's radius and ϕ is latitude. On a monthly mean basis, $\frac{\partial \bar{T}}{\partial t}$ is expected to be small, and QRL reflects the changes in temperature (Wehrbein & Leovy, 1982), so we have:

$$QRL = -(Q_{dyn} + QRS) \tag{2}$$

where:

$$Q_{dyn} = -w^* S - v^* \frac{\partial \bar{T}}{a \partial \phi} \tag{3}$$

Our model results suggest that changes in dynamics (which produce adiabatic cooling or warming) are the primary contributor to mesospheric temperature changes (Fig. 4). Although there are some regions where the difference in the mesospheric shortwave heating rate between the volcano case and control case is significant, changes in shortwave heating rate in response to the volcanic eruption are negligible with respect to other terms in Eq. (1).

The mean meridional circulation determines Q_{dyn} in the mesosphere. Following the HTHH eruption, there was a ∼20% strengthening of the mesospheric mean meridional circulation, which peaked in August of 2022, as shown by the red arrows in Fig. 5c. The polar winter SH shows strongly enhanced descending motion of ∼0.003 ms^{-1} between 0.1 hPa and 0.01 hPa, corresponding to the warm temperature anomaly seen in Fig. 3. In the summer Northern Hemisphere (NH), there is a weak acceleration in the ascending motion of ∼0.002 ms^{-1} above 0.1 hPa. In the tropical regions of both hemispheres, the horizontal mean flow accelerates by ∼1 ms^{-1} at around 0.1 hPa. The acceleration

of the mesospheric circulation in the tropics and the summer hemisphere coincides with the V-shaped region of cooling there (Fig. 2).

We attribute the strengthening of the mean meridional circulation in the mesosphere to the strengthening of the stratospheric westerlies, and their resultant effects on filtering vertically propagating gravity waves. As mentioned by Coy et al. (2022) and Wang et al. (2022), the stratospheric westerlies undergo strengthening and an equatorward shift in SH winter 2022, and this is also what we find in the ensemble of the volcanic simulations (see Fig. 5f). These stratospheric zonal wind changes are in balance with reduced planetary wave EP flux divergences (Fig. 5l). Changes in the stratospheric westerlies are consistent with the geostrophic wind that is derived from the meridional temperature gradient (Harvey et al., 2022; Holton, 2004, p.200) The strengthening of the stratospheric westerly jet between about 20°S and 60°S filters eastward propagating gravity waves in the (parameterized) gravity wave spectrum. This, in turn, enhances the net westward momentum flux reaching the mesosphere. As a result, westward gravity wave drag increases above 0.1 hPa (i.e., the drag becomes more negative, Fig. 5i), which accelerates the mesospheric meridional circulation in SH mid-latitudes above the region where the stratospheric westerlies have intensified (Fig. 5c). Although the forcing due to planetary waves in the mid-latitudes of the SH mesosphere weakens, as shown by the reduced (less negative) EP-flux divergence in Fig. 5l, it offsets only partially the increase in westward momentum deposited by the stronger gravity wave breaking. The combination of gravity wave drag and EP flux divergence produces a negative forcing anomaly (Fig. 5o) that is consistent with the acceleration of the meridional circulation seen in Fig. 5c.

The effect of the changes in the mean meridional circulation is reflected in the pattern of Q_{dyn} in the SH mid-latitudes shown in Fig. 4c. The acceleration of the meridional circulation in the SH mid-latitudes extends across the tropics and into the NH, showing a pattern similar to that found during interhemispheric coupling events, along with concomitant changes in temperature and zonal wind (cf. Smith et al., 2020, their Fig.4). Changes in gravity wave drag are also reflected in changes in the mesospheric zonal wind (Fig. 5f) since wave drag tends to accelerate or decelerate the mean flow toward the wave phase speed. An increase in the westward wave drag between 0.1 – 0.2 hPa in the subtropics leads to a weakening of the eastward zonal wind of $\sim$10 ms^{-1} there.

4 Discussion

In 2022, SABER stratospheric and mesospheric temperatures exhibited statistically significant changes, with record highs and lows observed in the stratosphere and mesosphere in August. Our study, based on fully-coupled simulations carried out with WACCM, shows good agreement with the observed temperature anomalies in the mesosphere. The model suggests the temperature anomalies in the mesosphere are a result of a global strengthening of the mesospheric meridional circulation of $\sim$20%. Through our analysis of the model, we have found that the changes in mesospheric dynamics observed in response to the HTHH volcanic eruption can be linked to dynamical changes occurring in the stratosphere, such as the strengthening of the westerlies, altered gravity wave propagation, the weakening of planetary wave dissipation, and the weakening of the Brewer-Dobson circulation.

The causal relationship between strengthening of the stratospheric westerlies and the mesospheric temperature anomalies is robust. In all the strong cases of the WACCM volcanic ensemble where the temperature field tripolar structure has an amplitude comparable to the observations, there is a strong strengthening and equatorward shift of the stratospheric westerlies, and in all the weak cases the stratospheric westerlies strengthen only weakly (Fig. 3). The timing of the strongest response in the mesosphere in 2022 also indicates that changes in the stratosphere are the cause of the changes in the mesosphere. The mesospheric circulation is strongest near the solstice, while in June the tem-

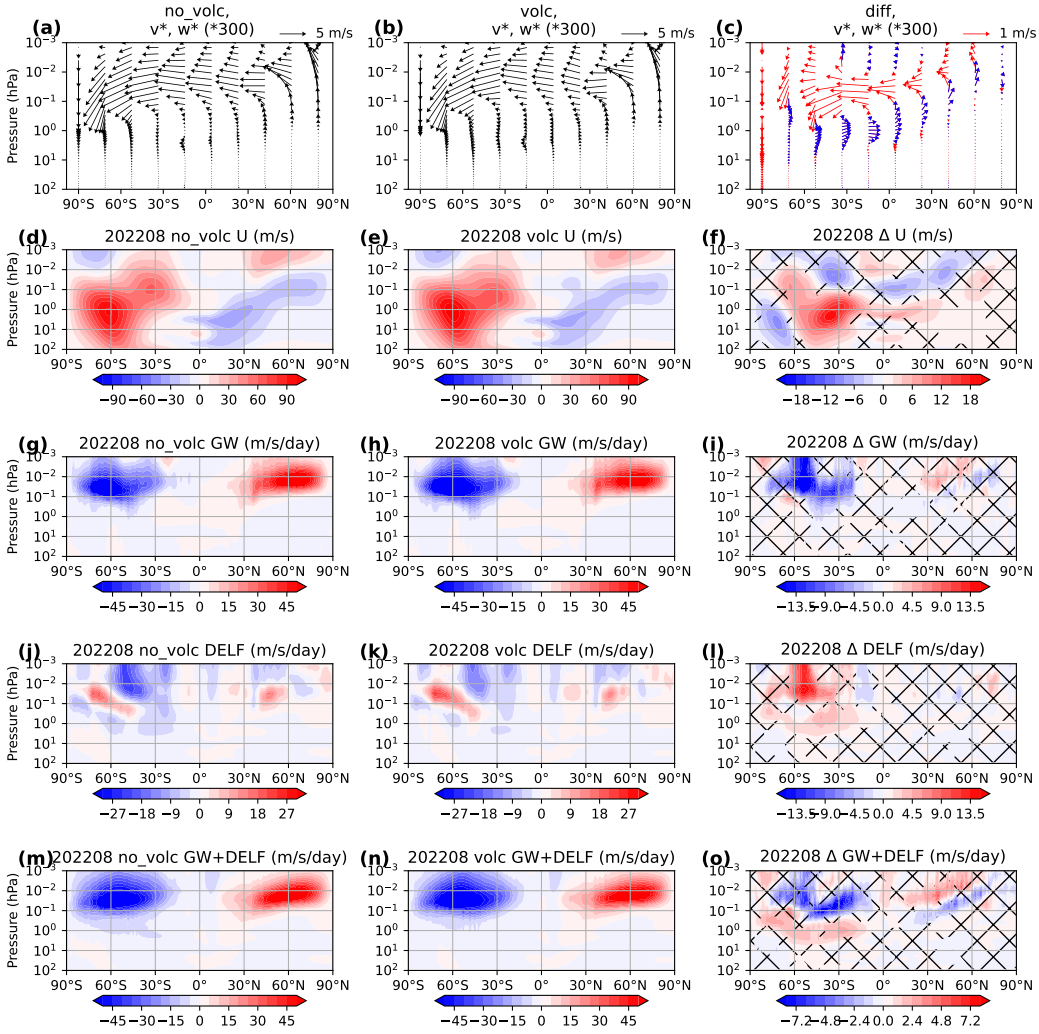

Figure 5. Zonal mean distribution of the WACCM 10-member ensemble mean for various quantities in August of 2022. (a-c) TEM circulation vectors (v^* and 300 × w^* for scaling), (d-f) zonal wind, (g-i) gravity wave drag, (j-l) EP-flux divergence, and (m-o) gravity wave drag plus the EP-flux divergence. The left column shows the control case, the middle column shows the volcano case, and the right column shows the difference between the volcano case minus the control case, where the areas with differences that have a p-value > 0.05 in a t-test are indicated by hatching. In (c), red arrows indicate a strengthening of the mean meridional velocity vector and blue arrows indicate a weakening thereof compared to the control case.

perature difference is insignificant. The strongest mesospheric temperature response occurs in August when the strengthening of the westerlies is largest in the stratosphere. It is also worth mentioning that in early 2023 neither the model nor the observations show a strong disturbance in stratospheric westerlies, or in the mesospheric temperature and circulation.

Since what happens in the mesosphere is a response to changes in the stratosphere, there are questions regarding changes in stratospheric dynamics itself. The facts that (1) not every member of the ensemble reproduces well the observed changes, and (2) the ensemble members that reproduce most closely the observed changes are not the same in July and August suggest that there is a stochastic component in the model results. We also attempted to find precursors for the changes in the stratosphere (radiative forcing, EP fluxes, meridional and zonal winds, tropical and subtropical temperatures), but were unable to find any statistically significant precursors for the large, significant changes that take place in July and August in the strong group of volcano ensemble members.

There remain many unsolved questions related to the abrupt changes seen in the stratosphere after the HTHH eruption. For example, what is the initial driver for the strong reduction of the SH planetary wave drag in the stratosphere in July and August? Is it the injected water vapor or the aerosols, or something else? Coy et al. (2022) suggested that the changes before June are due to the injected water vapor. As shown in our Fig. 2, there is a significant cooling in the stratosphere collocated with the injected water vapor anomaly before June. However, starting in June, a large, negative stratospheric temperature anomaly develops in the midlatitudes of the SH over a much broader altitude range. Since this anomaly is no longer collocated with the water vapor anomaly, it must be due to dynamical changes. However, as noted above, we were unable to identify any precursors to these changes. In addition, it is unclear why the stratospheric wind and circulation anomalies intensify suddenly in July and August. While the investigation of these stratospheric questions is outside the scope of our paper, addressing them would enhance our understanding of middle atmospheric dynamics and provide further insights into the HTHH volcanic eruption.

5 Open Research

- [Dataset] SABER v2.07 and v2.08 temperature data are available from `https://saber.gats-inc.com/data_services.php`, See Mlynczak et al. (2023)

- [Software] CESM2-WACCM6 codes are available from `//www.cesm.ucar.edu/models/cesm2`. See Gettelman et al. (2019).

Acknowledgments

WY, RG, JY, and MM are supported by the TIMED/SABER mission from the NASA Heliophysics Division. WY and JY are also supported by NASA's Heliophysics Division AIM mission and NSF AGS1901126. RG is supported in part by NASA grant 80NSSC19K1214. ZQ is supported by NSF AGS-1828589. The National Center for Atmospheric Research is sponsored by the National Science Foundation. Work conducted at CIRES/NOAA is supported by the NOAA's Earth Radiation Budget (ERB) Initiative (CPO #03-01-07-001), and in part by NOAA cooperative agreements NA17OAR4320101 and NA22OAR4320151. We thank Dr. James Russell III for his support and encouragement as an advisor at HU, and thank National Center for Atmospheric Research (NCAR) Atmospheric Chemistry Observations & Modeling (ACOM) for hosting WY's visit during this work. NCAR is sponsored by the U.S. National Science Foundation (NSF). WACCM is a component of the Community Earth System Model (CESM), which is supported by NSF and the Office of Science of the U.S. Department of Energy. Computing resources for the results presented here were provided by NCAR's Climate Simulation Laboratory, sponsored by

NSF and other agencies, and enabled by the computational and storage resources of NCAR's Computational and Information Systems Laboratory (CISL).

References

Andrews, D. G., Holton, J. R., & Leovy., C. B. (1987). *Middle atmosphere dynamics. no. 40. academic press, 1987.* Academic Press.

Carn, S. A., Krotkov, N. A., Fisher, B. L., & Li, C. (2022). Out of the blue: Volcanic so2 emissions during the 2021–2022 eruptions of hunga tonga—hunga ha'apai (tonga). *Frontiers in Earth Science*, *10*. Retrieved from https://www.frontiersin.org/articles/10.3389/feart.2022.976962 doi: 10.3389/feart.2022.976962

Coy, L., Newman, P. A., Wargan, K., Partyka, G., Strahan, S. E., & Pawson, S. (2022). Stratospheric circulation changes associated with the hunga tonga-hunga ha'apai eruption. *Geophysical Research Letters*, *49*(22), e2022GL100982. Retrieved from https://onlinelibrary.wiley.com/doi/abs/10.1029/2022GL100982 doi: 10.1029/2022GL100982

Dawkins, E. C., Feofilov, A., Rezac, L., Kutepov, A. A., Janches, D., Höffner, J., ... Russell, J. (2018). Validation of saber v2.0 operational temperature data with ground-based lidars in the mesosphere-lower thermosphere region (75–105 km). *Journal of Geophysical Research: Atmospheres*, *123*(17), 9916–9934. doi: 10.1029/2018JD028742

Dunkerton, T. (1978, 12 1). On the mean meridional mass motions of the stratosphere and mesosphere. *Journal of the Atmospheric Sciences*, *35*(12), 2325–2333. Retrieved from https://journals.ametsoc.org/view/journals/atsc/35/12/1520-0469_1978_035_2325_otmmmm_2_0_co_2.xml doi: 10.1175/1520-0469(1978)035{\textless}2325:OTMMMM{\textgreater}2.0.CO;2

Garcia, R. R., & Solomon, S. (1985). The effect of breaking gravity waves on the dynamics and chemical composition of the mesosphere and lower thermosphere. *Journal of Geophysical Research*, *90*(D2), 3850. Retrieved from http://doi.wiley.com/10.1029/JD090iD02p03850 doi: 10.1029/JD090iD02p03850

García-Comas, M., López-Puertas, M., Marshall, B. T., Wintersteiner, P. P., Funke, B., Bermejo-Pantaleón, D., ... Russell III, J. M. (2008). Errors in sounding of the atmosphere using broadband emission radiometry (saber) kinetic temperature caused by non-local-thermodynamic-equilibrium model parameters. *Journal of Geophysical Research: Atmospheres*, *113*(D24). Retrieved from https://onlinelibrary.wiley.com/doi/abs/10.1029/2008JD010105 doi: 10.1029/2008JD010105

Gettelman, A., Mills, M. J., Kinnison, D. E., Garcia, R. R., Smith, A. K., Marsh, D. R., ... Randel, W. J. (2019). The whole atmosphere community climate model version 6 (waccm6). *Journal of Geophysical Research: Atmospheres*, *124*(23), 12380–12403. doi: 10.1029/2019JD030943

Harvey, V. L., Pedatella, N., Becker, E., & Randall, C. (2022, 8 16). Evaluation of polar winter mesopause wind in waccmx+dart. *Journal of Geophysical Research: Atmospheres*, *127*(15). Retrieved from https://onlinelibrary.wiley.com/doi/10.1029/2022JD037063 doi: 10.1029/2022JD037063

Holton, J. R. (1983, 10 1). The influence of gravity wave breaking on the general circulation of the middle atmosphere. *Journal of the Atmospheric Sciences*, *40*(10), 2497–2507. Retrieved from https://journals.ametsoc.org/view/journals/atsc/40/10/1520-0469_1983_040_2497_tiogwb_2_0_co_2.xml doi: 10.1175/1520-0469(1983)040<2497:TIOGWB>2.0.CO;2

Holton, J. R. (2004). *An introduction to dynamic meteorology* (4th ed.; R. Dmowska & J. R. Holton, Eds.). Burlington, MA: Elsevier Academic Press,. Retrieved from http://books.google.com/books?id=fhW5oDv3EPsC

Holton, J. R., & Mass, C. (1976, 11 1). Stratospheric vacillation cycles. *Journal of the Atmospheric Sciences*, *33*(11), 2218–2225. Retrieved from https://journals.ametsoc.org/view/journals/atsc/33/11/1520-0469_1976_033_2218_svc_2_0_co_2.xml doi: 10.1175/1520-0469(1976)033{\textless}2218:SVC{\textgreater}2.0.CO;2

Khaykin, S., Podglajen, A., Ploeger, F., Grooß, J.-U., Tence, F., Bekki, S., ... Ravetta, F. (2022, 12 14). Global perturbation of stratospheric water and aerosol burden by hunga eruption. *Communications Earth & Environment*, *3*(1), 1–15. Retrieved from https://www.nature.com/articles/s43247-022-00652-x doi: 10.1038/s43247-022-00652-x

Lindzen, R. S. (1981). Turbulence and stress owing to gravity wave and tidal breakdown. *Journal of Geophysical Research*, *86*(C10), 9707. Retrieved from http://doi.wiley.com/10.1029/JC086iC10p09707 doi: 10.1029/JC086iC10p09707

Livesey, N. J., Read, W., Lambert, A., Cofield, R., Cuddy, D., Froidevaux, L., ... Co, R. E. (2020). *Earth observing system (eos) aura microwave limb sounder (mls) description document* (Tech. Rep.).

Millán, L., Santee, M. L., Lambert, A., Livesey, N. J., Werner, F., Schwartz, M. J., ... Froidevaux, L. (2022). The hunga tonga-hunga ha'apai hydration of the stratosphere. *Geophysical Research Letters*, *49*(13), e2022GL099381. Retrieved from http://onlinelibrary.wiley.com/doi/abs/10.1029/2022GL099381 doi: 10.1029/2022GL099381

Mlynczak, M. G., Daniels, T., Hunt, L. A., Yue, J., Marshall, B. T., Russell, J. M., ... Yee, J. H. (2020). Radiometric stability of the saber instrument. *Earth and Space Science*, *7*(2), e2019EA001011. doi: 10.1029/2019EA001011

Mlynczak, M. G., Marshall, B. T., Garcia, R. R., Hunt, L., Yue, J., Harvey, V. L., ... Russell, J. (2023, 3 16). Algorithm stability and the long-term geospace data record from timed/saber. *Geophysical Research Letters*, *50*(5). Retrieved from https://onlinelibrary.wiley.com/doi/10.1029/2022GL102398 doi: 10.1029/2022GL102398

Proud, S. R., Prata, A. T., & Schmauß, S. (2022, 11 4). The january 2022 eruption of hunga tonga-hunga ha'apai volcano reached the mesosphere. *Science*, *378*(6619), 554–557. Retrieved from http://www.science.org/doi/10.1126/science.abo4076 doi: 10.1126/science.abo4076

Randall, C. E., Harvey, V. L., Siskind, D. E., France, J., Bernath, P. F., Boone, C. D., & Walker, K. A. (2009). Nox descent in the arctic middle atmosphere in early 2009. *Geophysical Research Letters*, *36*(18). Retrieved from https://onlinelibrary.wiley.com/doi/abs/10.1029/2009GL039706 doi: 10.1029/2009GL039706

Randel, W. J., Johnston, B. R., Braun, J. J., Sokolovskiy, S., Vömel, H., Podglajen, A., & Legras, B. (2023, 1). Stratospheric water vapor from the hunga tonga–hunga ha'apai volcanic eruption deduced from cosmic-2 radio occultation. *Remote Sensing*, *15*(8), 2167. Retrieved from https://www.mdpi.com/2072-4292/15/8/2167 doi: 10.3390/rs15082167

Randel, W. J., & Newman, P. A. (1998). The stratosphere in the southern hemisphere. In D. J. Karoly & D. G. Vincent (Eds.), *Meteorology of the southern hemisphere* (pp. 243–282). Boston, MA: American Meteorological Society. Retrieved from https://doi.org/10.1007/978-1-935704-10-2_9

Remsberg, E., Marshall, B. T., Garcia-Comas, M., Krueger, D., Lingenfelser, G. S., Martin-Torres, J., ... Thompson, R. E. (2008). Assessment of the quality of the version 1.07 temperature-versus-pressure profiles of the middle atmosphere from timed/saber. *Journal of Geophysical Research: Atmospheres*, *113*(D17), 17101. doi: 10.1029/2008JD010013

Rienecker, M., Suarez, M., Todling, R., Bacmeister, J., Takacs, L., Liu, H.-C., ... Nielsen, J. (2018). *The geos-5 data assimilation system— documentation of*

versions 5.0.1, 5.1.0, and 5.2.0 (Tech. Rep.).

Russell, J. M., Mlynczak, M. G., Gordley, L. L., Tansock, J. J., Jr., & Esplin, R. W. (1999, 10 20). Overview of the saber experiment and preliminary calibration results. In (Vol. 3756, p. 277). International Society for Optics and Photonics. Retrieved from https://www.spiedigitallibrary.org/conference-proceedings-of-spie/3756/0000/Overview-of-the-SABER-experiment-and-preliminary-calibration-results/10.1117/12.366382.full doi: 10.1117/12.366382

Schoeberl, M. R., Wang, Y., Ueyama, R., Taha, G., Jensen, E., & Yu, W. (2022). Analysis and impact of the hunga tonga-hunga ha'apai stratospheric water vapor plume. *Geophysical Research Letters*, *49*(20), e2022GL100248. Retrieved from https://onlinelibrary.wiley.com/doi/abs/10.1029/2022GL100248 doi: 10.1029/2022GL100248

Sellitto, P., Podglajen, A., Belhadji, R., Boichu, M., Carboni, E., Cuesta, J., ... Legras, B. (2022, 11 19). The unexpected radiative impact of the hunga tonga eruption of 15th january 2022. *Communications Earth & Environment*, *3*(1), 1–10. Retrieved from http://www.nature.com/articles/s43247-022-00618-z doi: 10.1038/s43247-022-00618-z

Smith, A. K., Garcia, R. R., Marsh, D. R., & Richter, J. H. (2011, 10 20). Waccm simulations of the mean circulation and trace species transport in the winter mesosphere. *Journal of Geophysical Research*, *116*(D20), D20115. Retrieved from http://doi.wiley.com/10.1029/2011JD016083 doi: 10.1029/2011JD016083

Smith, A. K., Marsh, D. R., Mlynczak, M. G., & Mast, J. C. (2010). Temporal variations of atomic oxygen in the upper mesosphere from saber. *Journal of Geophysical Research: Atmospheres*, *115*(D18). Retrieved from https://onlinelibrary.wiley.com/doi/abs/10.1029/2009JD013434 doi: 10.1029/2009JD013434

Smith, A. K., Pedatella, N. M., & Mullen, Z. K. (2020, 3 1). Interhemispheric coupling mechanisms in the middle atmosphere of waccm6. *Journal of the Atmospheric Sciences*, *77*(3), 1101–1118. Retrieved from https://journals.ametsoc.org/view/journals/atsc/77/3/jas-d-19-0253.1.xml doi: 10.1175/JAS-D-19-0253.1

Taha, G., Loughman, R., Colarco, P. R., Zhu, T., Thomason, L. W., & Jaross, G. (2022). Tracking the 2022 hunga tonga-hunga ha'apai aerosol cloud in the upper and middle stratosphere using space-based observations. *Geophysical Research Letters*, *49*(19), e2022GL100091. Retrieved from http://onlinelibrary.wiley.com/doi/abs/10.1029/2022GL100091 doi: 10.1029/2022GL100091

Vincent, R. A. (2015, 3). The dynamics of the mesosphere and lower thermosphere: a brief review. *Progress in Earth and Planetary Science*, *2*(1), 4. Retrieved from http://www.progearthplanetsci.com/content/2/1/4 doi: 10.1186/s40645-015-0035-8

Vömel, H., Evan, S., & Tully, M. (2022, 9 23). Water vapor injection into the stratosphere by hunga tonga-hunga ha'apai. *Science*, *377*(6613), 1444–1447. Retrieved from https://www.science.org/doi/full/10.1126/science.abq2299 doi: 10.1126/science.abq2299

Wang, X., Randel, W., Zhu, Y., Tilmes, S., Starr, J., Yu, W., ... Li, J. (2022, 11 26). *Stratospheric climate anomalies and ozone loss caused by the hunga tonga volcanic eruption* (Tech. Rep.). Retrieved from https://essopenarchive.org/doi/full/10.1002/essoar.10512922.1

Waters, J. W., Froidevaux, L., Harwood, R. S., Jarnot, R. F., Pickett, H. M., Read, W. G., ... Walch, M. J. (2006, 5). The earth observing system microwave limb sounder (eos mls) on the aura satellite. *IEEE Transactions on Geoscience and Remote Sensing*, *44*(5), 1075–1092. doi: 10.1109/TGRS.2006.873771

Wehrbein, W. M., & Leovy, C. B. (1982, 7 1). An accurate radiative heating and cooling algorithm for use in a dynamical model of the middle atmosphere. *Journal of the Atmospheric Sciences*, *39*(7), 1532–1544. Retrieved from `https://journals.ametsoc.org/view/journals/atsc/39/7/1520-0469_1982_039_1532_aarhac_2_0_co_2.xml` doi: 10.1175/1520-0469(1982)039{\textless}1532:AARHAC{\textgreater}2.0.CO;2

Zhu, Y., Bardeen, C. G., Tilmes, S., Mills, M. J., Wang, X., Harvey, V. L., ... Toon, O. B. (2022, 10 22). Perturbations in stratospheric aerosol evolution due to the water-rich plume of the 2022 hunga-tonga eruption. *Communications Earth & Environment*, *3*(1), 1–7. Retrieved from `https://www.nature.com/articles/s43247-022-00580-w` doi: 10.1038/s43247-022-00580-w